Geomechanics and Engineering, *Vol. 31, No. 4 (2022) 365-373*
https://doi.org/10.12989/gae.2022.31.4.365

Damage characterization of hard-brittle rocks under cyclic loading based on energy dissipation and acoustic emission characteristics

Cheng J. Li[1,2], Pei J. Lou*[2,3] and Ying Xu[1,2,3]

[1]*State Key Laboratory of Mining Response and Disaster Prevention and Control in Deep Coal Mine, Anhui University of Science and Technology, Huainan, Anhui 232001, China*
[2]*School of Civil Engineering and Architecture, Anhui University of Science and Technology, Huainan, Anhui 232001, China*
[3]*Engineering Research Center of Underground Mine Construction, Ministry of Education, Anhui University of Science and Technology, Huainan, Anhui 232001, China*

(*Received May 1, 2020, Revised September 7, 2022, Accepted September 14, 2022*)

Abstract. In order to investigate the damage evolution law of rock specimens under cyclic loading, cyclic loading tests under constant loads with different amplitudes were carried out on limestone specimens with high strength and brittleness values using acoustic emission (AE) technology and the energy evolution and AE characteristics were evaluated. Based on dissipated energy density and AE counts, the damage variable of specimen was characterized and two damage evolution processes were analyzed and compared. The obtained results showed that the change of AE counts was closely related to radial deformation. Higher cyclic loading values result in more significant radial strain of limestone specimen and larger accumulative AE counts of cyclic loading segment, which indicated Felicity effect. Regarding dissipated energy density, the damage of limestone specimen was defined without considering the influence of radial deformation, which made the damage value of cyclic loading segment higher at lower amplitude loads. The damage of cyclic loading segment was increased with the magnitude of load. When dissipated energy density was applied to define damage, the damage value at unloading segment was smaller than that of AE counts. Under higher cyclic loading values, rocks show obvious damage during both loading and unloading processes. Therefore, during deep rock excavation, the damages caused by the deformation recovery of unloading rocks could not be ignored when considering the damage caused by abutment pressure.

Keywords: AE counts, cyclic loading, damage variable, energy dissipation, residual strain

1. Introduction

The rapid development of social economy has greatly increased the scale of underground engineering constructions. The stability of surrounding rock masses is indispensable for smooth underground engineering excavations and the safety and reliability of underground space constructions. Rock materials have original defects and excavation aggravates the damage of surrounding rock masses. The damage degree of rock masses determines their bearing capacity and reasonable characterization of rock damage evolution process is helpful in judging and controlling the stability of underground engineering. At present, many researchers are studying the damage law of rocks during deformation under loading (Srinivasan *et al.* 2020, Diederichs *et al.* 2004, Ghamgosar *et al.* 2017). Generally speaking, there are two types of damage characterization methods. The first one relies on the physical and mechanical parameters of rock materials, including elastic modulus (Xiao *et al.* 2010), residual strain (Xiao *et al.* 2011), fracture volume strain (Qiu *et al.* 2014), energy density (Liu *et al.* 2016, Min *et al.* 2020), etc. These parameters can generally be obtained from the stress-strain curve of rock specimens. The second one is to realize damage characterization by measuring the physical and chemical phenomena associated with rock deformation and failure processes, such as AE (Tang *et al.* 2020, Castagna *et al.* 2018), acoustic wave (Wang *et al.* 2008), resistance (Wang *et al.* 2012), infrared radiation (Xiao *et al.* 2019), electromagnetic radiation (Jin *et al.* 2013), CT (Zhou *et al.* 2008), etc. The damage change of rocks during loading is a dynamic evolution process. The characteristics of rock specimen deformation and failure cause some parameter changes to only represent a single aspect of damage process, which has certain limitations and cannot truly reflect the comprehensive damage of the specimen as a whole. Therefore, damage evolution patterns determined by different parameters are different (Kim *et al.* 2015). Rational damage characterization methods have to be determined after comprehensive comparisons based on the actual situations of rock deformation and damage.

However, the stress states of surrounding rock masses in engineering excavations are complicated, which are often under cyclic loads (Chen *et al.* 2016, Fuenkajorn and Phueakphum 2010). For example, the periodic storage and drainage of reservoirs exposes dam foundations to loading and unloading cycles. The surrounding rock masses of the transportation roadways in mining areas are also affected by cyclic loadings during the progress of working faces in upper and lower mining areas. Therefore, many researchers

*Corresponding author, Ph.D.
E-mail: pjlou@aust.edu.cn

ISSN: 2005-307X (Print), 2092-6219 (Online)

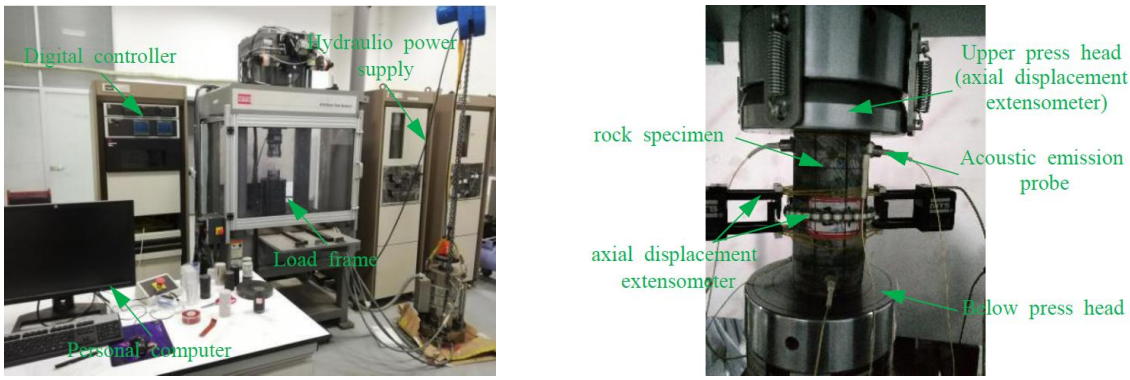

(a) MTS rock mechanical test system (b) AE probe fixing

Fig. 1 Standard limestone specimen and AE probe installation

have studied the mechanical and damage characteristics of complex stress loading processes of rocks (Voznesenskii *et al.* 2016, Chu *et al.* 2019, Li *et al.* 2020). The results have shown that the fatigue strength of rock is generally lower than its uniaxial strength, and limit strain is greater than peak strain under uniaxial loading, which indicates that the damage of specimens under cyclic loading is a process of slow accumulation with the increase of cycle number (Peng *et al.* 2019). Xiao *et al.* (2010) characterized the damage evolution of granite specimens from multiple perspectives, such as residual strain, energy, AE, etc., and found that the damage variable of specimens changed in an inverted "S" shape with cycle number. Xiao *et al.* (2011) drew similar conclusions through the analysis of the damage variable of rock salt, which showed that there were certain relationships among different parameters in the damage process of specimens. However, there were still some differences in the damage changes of rock specimens under cyclic loadings with different parameter values (Liu *et al.* 2018). It was found that, unlike hard-brittle rocks, the rock specimens used in above experiments showed obvious viscous or plastic characteristics. In recent years, with the continuous progress of underground engineering constructions, there have been frequent disasters such as rock bursts and coal bumps (Naji *et al.* 2018, Qi and Ma 2019). Rock masses in which rock bursts take place often present strong elastic brittle characteristics, therefore, it is of great significance to study the damage evolution of rocks with higher brittleness under cyclic loading.

The limestone specimen tested in this study had obvious elastic brittle characteristics, which was similar to the mechanical characteristics of rock masses with rock burst tendency at the engineering site. Considering the stress-strain curve of limestone specimen, it was more suitable to define damage in terms of energy than other physical and mechanical parameters. Then, the energy dissipation and AE characteristics of the specimen were also analyzed. The damage of the specimen was characterized by the change of dissipated energy density and AE counts and damage evolution law was analyzed comparatively, especially damage evolution mechanisms during both loading and unloading processes.

2. Summary of constant amplitude cyclic loading test scheme

The limestone rock specimens tested in this study were collected from Gubei Mine in Huainan, China. The cores were processed into standard cylindrical specimens of Φ50×100 mm in laboratory, as shown in Fig. 1(a). The measured average acoustic wave velocity was 5.03×10^3 m/s, density was 2.73×10^3 kg/m^3, elastic modulus was 28.81 GPa, uniaxial strength was 161.30 MPa, and Poisson's ratio was 0.10. Compression tests were performed on MTS816 of Anhui University of Science and Technology. Axial and radial displacements were measured by axial displacement extensometer and circumferential strain gauge placed on the specimen, respectively. PCI-2 AE test and analysis system produced by American Physical Acoustics Corporation (PAC) was adopted for AE tests. During the test, six channels were used for data collection. Each channel corresponded to an independent preamplifier and sensor. The threshold value of sensors was set to 40 dB. AE probe was attached to the surface of specimen by Vaseline, as shown in Fig. 1(b).

The research showed that when the peak load reached a certain level, the sensitivity of specimen to cyclic loading was greatly increased (Liu *et al*. 2018). In order to set a reasonable value to evaluate specimen responses to cyclic loadings with different stress levels, especially the deformation and failure characteristics of the specimen near ultimate load, three cyclic loading amplitudes of 70, 115 and 160 MPa were set as the upper limit and the lower limit was fixed at 30 MPa as to avoid the influence of pore fracture compaction segment on test analysis, that is, the amplitudes of cyclic loading were 40, 85 and 130 MPa, respectively. The loading and unloading rates of uniaxial compression and cyclic loading were set to 1 kN/s. Loading and unloading segments formed a cycle and the cycle number of each amplitude was set to 10. After 10 cycles, specimens were loaded to failure at the same rate. Due to the inevitability of the strength dispersion of specimens, some specimens could not successfully achieve cyclic loading under 130 MPa, therefore, multiple specimens were prepared for testing.

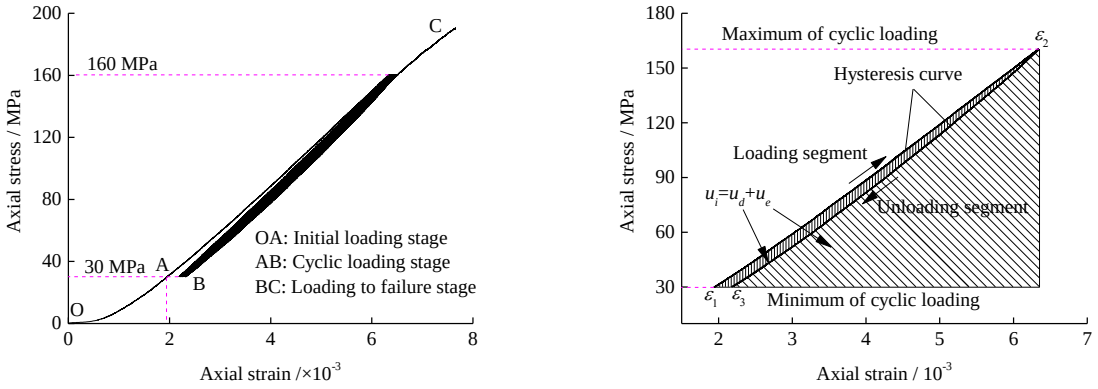

(a) Three stages of stress-strain curve under cyclic load (b) Elastic energy density and dissipated energy density

Fig. 2 Calculation of the energy density of specimens during cyclic loading

3. Results and analysis

3.1 Energy dissipation of limestone specimens

The deformation and failure processes of rock specimens under compression are energy evolution processes (Xie *et al.* 2009). Some part of the energy applied by press to specimen was converted into elastic energy of specimens and stored, which could be recovered during unloading, and the other part was mainly used for the irreversible deformation of specimen. For limestone specimens with elastic and brittle characteristics, the energy of rock element under uniaxial load was expressed as

$$\begin{cases} u_i = u_e + u_d \\ u_i = \int \sigma \mathrm{d}\varepsilon \\ u_e = \sigma^2 / 2E \end{cases} \quad (1)$$

where u_i is input energy density, u_e is elastic energy density, and u_d is dissipated energy density, all in terms of J/cm^3.

The energy density of specimens under cyclic loading was different from that under uniaxial loading. As shown in Fig. 2(a), taking the amplitude 130 MPa as an example, calculations had to be divided into three stages, namely initial loading stage, cyclic loading segment and loading to failure segment. OA and BC segments were calculated according to Eq. (1) and elastic modulus values were obtained from the slope of the linear elastic segments of cyclic loading curves. The unloading segment of cyclic loading is the result of energy release. Dissipated energy density cannot be solved with Eq. (1). Therefore, the dissipated energy density of AB segment had to be obtained through the integral of loading and unloading curves, as shown in Fig. 2(b), using the following equation

$$\begin{cases} u_i = \int_{\varepsilon_1}^{\varepsilon_2} \sigma \mathrm{d}\varepsilon \\ u_d = u_i - u_e \\ u_e = \int_{\varepsilon_2}^{\varepsilon_3} \sigma \mathrm{d}\varepsilon \end{cases} \quad (2)$$

where ε_1 and ε_3 are strains at lower limits before and after loading and unloading process and ε_2 is strain at the upper limit of cyclic loading.

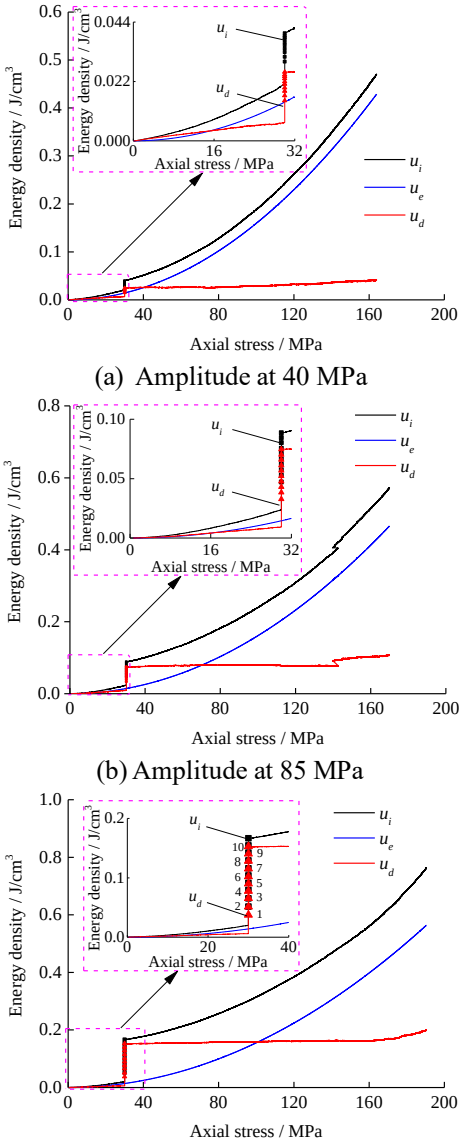

(a) Amplitude at 40 MPa

(b) Amplitude at 85 MPa

(c) Amplitude at 130 MPa

Fig. 3 Energy density evolution under different amplitudes of 40, 85 and 130 MPa

Three types of energy density changes of the whole

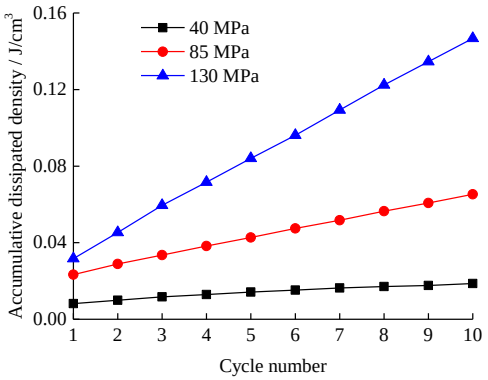

Fig. 4 The variation of accumulated dissipated energy density at cyclic loading stage with cycle number

loading and unloading process of the specimens in cyclic loading tests were obtained using Eqs. (1) and (2), as shown in Fig. 3. In initial loading stage, specimens were in micropore fracture compaction stage and the plastic deformation produced by compaction process was larger, therefore, the increase of u_d was more significant. The average values of u_d and u_e at three amplitudes of 40, 85 and 130 MPa were obtained to be 7.31×10^{-3} and 1.43×10^{-2} J/cm^3 at this stage. When loads were below 15 MPa, u_d was greater than u_e. Cyclic loading segments generated dissipated energy in each cycle and the overall dissipated energy density was increased with load amplitude in this stage. The overall dissipated energy density under cyclic loads of 40, 85 and 130 MPa were 1.87×10^{-2}, 6.55×10^{-2} and 14.67×10^{-2} J/cm^3, respectively. When axial stress was lower than the upper limit of cyclic loading, there was little dissipated energy in specimens during failure stage and specimens exhibited strain hardening characteristics. However, dissipated energy was obviously increased until specimen failure at stress values of close to the peak value. Under cyclic loads of 40, 85 and 130 MPa, u_i values were 0.470, 0.573 and 0.764 J/cm^3, and u_d values were 0.042, 0.106 and 0.201 J/cm^3, respectively. Based on these values, the corresponding ratios of u_d to u_i were 0.089, 0.185 and 0.263, respectively. It was seen that, higher amplitudes of cyclic loading resulted in higher energy dissipation at specimen failure.

The variation of accumulated dissipated energy density u_d^a at cyclic loading stage with cycle number n is shown in Fig. 4. The dissipated energy produced in the initial cycle was higher than those of subsequent cycles under the same amplitude. Under the cyclic loading amplitude of 40 MPa, dissipated energy density u_d was gradually decreased in each cycle and u_d^a tended to be stable as n was increased. Under the cyclic loading amplitudes of 85 and 130 MPa, u_d^a was increased almost linearly with cycle number, which meant that when load amplitude was increased to a certain extent, each cycle, except the initial cycle, produced a certain amount of approximately equal dissipated energy and higher cyclic loading amplitudes increased growth rate. It could be predicted that, when cycle number reached a certain value under higher load amplitudes, the dissipated energy of specimens reached a certain limit value and specimens failed.

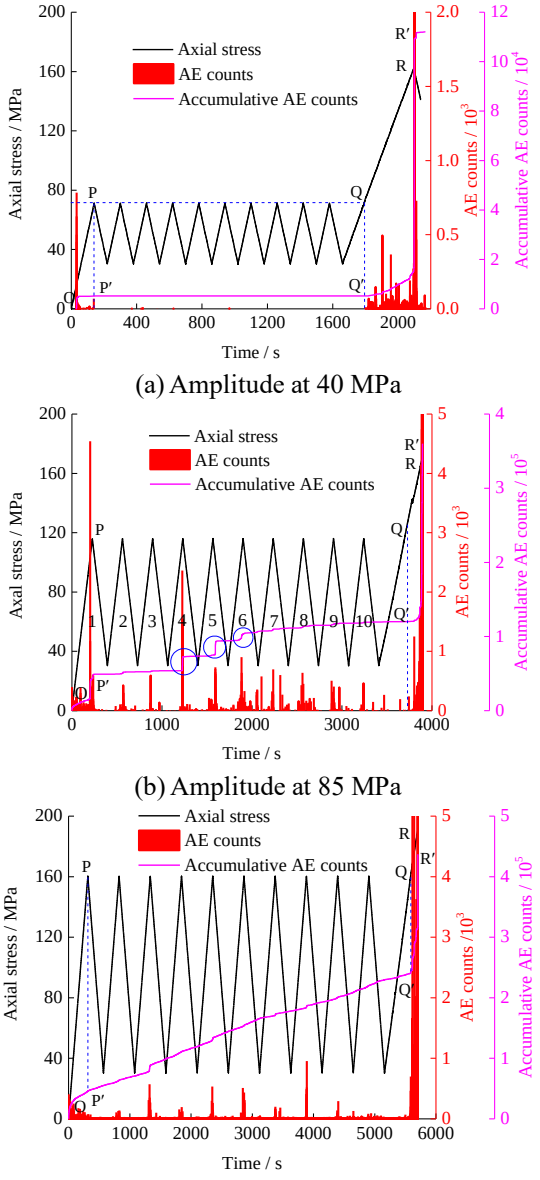

(a) Amplitude at 40 MPa

(b) Amplitude at 85 MPa

(c) Amplitude at 130 MPa

Fig. 5 Variation of axial stress, AE counts and accumulative AE counts with time

3.2 AE characteristics limestone specimen

AE phenomenon occurs during rock failure and AE characteristic parameters are closely related to damage (Kim *et al.* 2015). AE counts is defined as the number of signal oscillations exceeding the threshold value, which can be used for AE activity evaluation. Fig. 5 shows the variation of axial stress, AE counts and accumulative AE counts with time under different cyclic loads. At initial loading stage, a certain number of elastic waves were generated during the compaction of the pore cracks of specimens, which led to AE phenomena. At the amplitude of 40 MPa, cyclic loading segment rarely produced AE counts except for the loading segment in initial cycle. However, in loading to failure segment, AE counts began to occur in large numbers after stress reaching the upper limit of cyclic loading, showing a significant Kaiser effect

(Bahrani *et al.* 2019). The proportion of AE counts in cyclic loading segment to accumulative AE counts at specimen failure was only 0.2%.

At the amplitude of 85 MPa, AE phenomenon in cyclic loading segment was obviously enhanced and was mainly concentrated near the upper limit stress in the cycle, in which the proportion of AE counts was increased to 39.1%. Meanwhile, this phenomenon was observed in both loading and unloading segments. A large amount of AE counts were produced near the upper limit stress of the 4th and 5th cycles and then decreased with the increase of cycle number. When axial stress exceeded the upper limit of cyclic loading, AE counts began to significantly increase again.

At the amplitude of 130 MPa, the AE counts of the specimen at peak stress were greater than those at other stress levels in the same cycle. The AE counts of each cycle in this segment are basically equal to and larger than those obtained at the amplitude of 85 MPa. Except for the vicinity of peak load, generation rates at other stress levels were close, which increased accumulative AE counts almost linearly with time and the proportion of accumulative AE counts for cyclic loading segment was further increased, to 63.3%. It was seen that specimen had obvious felicity effect (Li *et al.* 2019), showing unstable deformation states.

Besides, it can be found that the maximum AE counts at the amplitude of 85 MPa is greater than those of 130 MPa. In fact, the AE counts are related to the elastic waves generated at a certain position inside the rock when it damaged. Defects such as micropores and cracks are common in rock materials, and relatively large elastic waves will be generated due to the "instability" in small parts of the specimen during loading. Due to the certain dispersion of rock specimens, the maximum AE counts at the amplitude of 85 MPa might be greater than those of 130 MPa. However, this phenomenon was only occasional, and according to the cumulative AE counts, the AE counts generated by each cycle at amplitude of 130MPa was greater than those of 85 MPa.

3.3 Damage characterization and evolution of specimens

Energy dissipation and AE characteristics of specimens are described in Sections 3.1 and 3.2. It was found that in specimen failure, both of the abovementioned characteristics showed certain regularity under cyclic loads. Dissipated energy density under different stress levels was normalized based on accumulative dissipated energy density at specimen failure and the relationship between rock damage and dissipated energy density was obtained as

$$D_e = u_d / u_d^t \tag{3}$$

where D_e is the damage variable characterized by dissipated energy density and u_d^t is accumulative dissipated energy density at specimen failure.

Similarly, accumulative AE counts were used to normalize AE counts under different stress conditions as

$$D_a = N / N_a \tag{4}$$

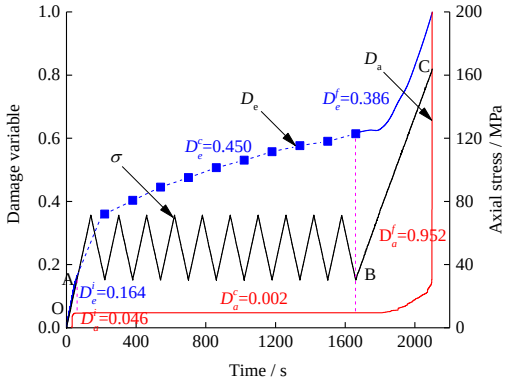

(a) Amplitude at 40 MPa

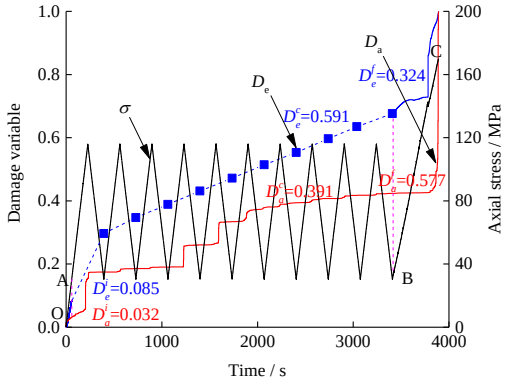

(b) Amplitude at 85 MPa

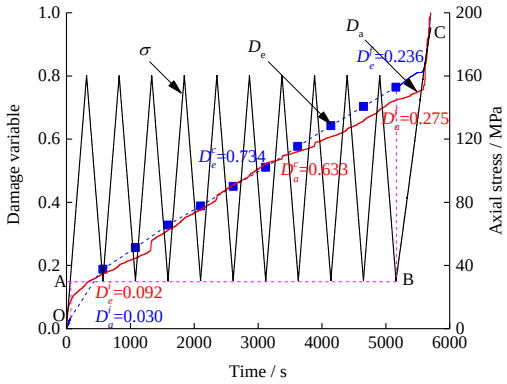

(c) Amplitude at 130 MPa

Fig. 6 Damage characterization based on dissipated energy density and AE counts

where D_a is the damage variable characterized by accumulative AE counts, N is AE counts under any stress, and N_a is accumulative AE counts at specimen failure. The variation of two types of damage variables with time at the amplitudes of 40, 85, and 130 MPa is shown in Fig. 6.

When damage is defined by dissipated energy density, it cannot reflect the damage value of cyclic loading segment at any stress state. Therefore, Fig. 6 only presents damage values in each complete cycle for 10 cycles. D_e^i, D_e^c and D_e^f represent three segments of damage defined by dissipated energy density and D_a^i, D_a^c and D_a^f represent three segments of damage defined by AE counts, respectively. Obviously, the variation trends of specimen damage with time characterized by the two methods were consistent with accumulative dissipated energy density or accumulative AE

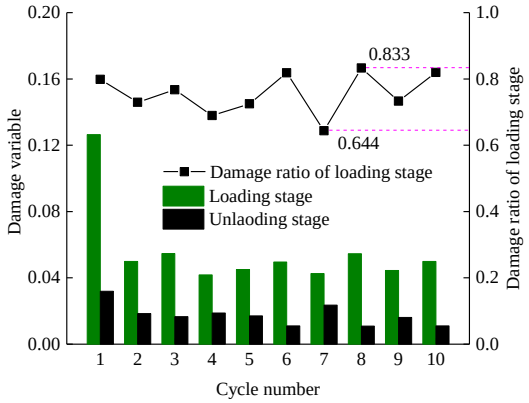

(a) Damage variable characterized by dissipated energy density

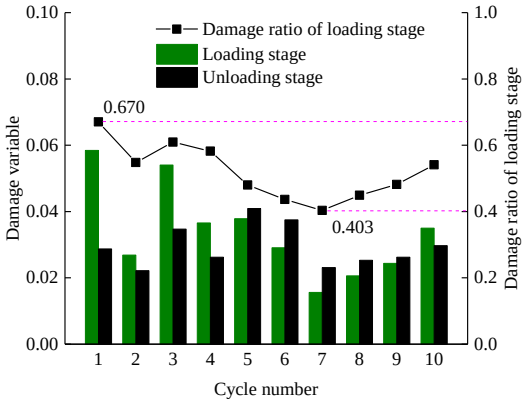

(b) Damage variable characterized by AE counts

Fig. 7 Damage change of loading and unloading segments at the amplitude of 130 MPa

counts. In Section 3.2, the variation rules of dissipated energy density and AE counts have been analyzed, therefore, it is not necessary to describe the damage trends of three segments in detail here and corresponding damage value is shown in Fig. 6. In the following sections, a comparative analysis of damage evolution process characterized by the two methods is performed.

At the amplitude of 40 MPa, D_e was greater than D_a during the whole process of specimen deformation and failure. The damage variables of initial and cyclic loading segments defined by AE counts were very small and damage mainly occurred in loading to failure segment where damage speed was rapidly increased near failure. As for the damage variable defined by dissipated energy density, D_e^c was the largest in the three segments and the damage in each cycle was decreased with the increase of cycle number. At cyclic loading amplitude of 85 MPa, D_e was still higher than D_a, but its values were closer to each other than those at the amplitude of 40 MPa. For damages defined by AE counts at this amplitude load, D_a^f was still the largest, D_a^c was significantly increased while using dissipated energy density for definition, and D_e^c was the largest and increased compared to that at the amplitude of 40 MPa. At the amplitude of 130 MPa, the two damage processes were basically the same and damage mainly occurred in cyclic loading segment. Actually, whether using the definition of dissipated energy density or AE counts, the larger the cyclic loading amplitude, the smaller the proportion of damage in the initial loading segment, and the larger the proportion of damage in cyclic loading section. At the amplitude of 130 MPa, the variation of AE counts in each cycle was stable, and the differences of dissipated energy density in each cycle were small. Therefore, the damage under the two definitions gradually approaches as the amplitude of cyclic loading increases. It was also easily found that the increasing speed of D_a^f at this amplitude was smaller than those of the two lowest amplitudes when specimens were near failure.

In general, with increasing of the amplitude of cyclic loading, the damage of cyclic loading segment was gradually increased under the two definition approaches, while the damage in loading to failure segment was gradually decreased. When AE counts were used for definition, the damage variations were more significant in these two segments. It is worth noting that the magnitudes of damage variable D for different specimens did not represent the magnitudes of dissipated energy or AE counts and it was just a reflection of the damage process of each specific specimen, because damage definition was based on the specimen themselves. In other words, under the same damage variable, the damage degrees of specimens under different amplitudes were not the same. Therefore, damage variables at different amplitudes could not be compared.

The above damage in cyclic loading segment defined by dissipated energy density represented the damage in every whole cycle, while the damage change at any time was reflected when AE counts were used for characterization, AE phenomenon showed that both loading and unloading processes produced damage. In fact, dissipated energy density u_d^l in loading cyclic loading segment was calculated using Eq. (1). Then, dissipated energy density in unloading segment was obtained using the following formula

$$u_d^u = u_d^t - u_d^l \tag{5}$$

where u_d^u and u_d^t are dissipated energy density in unloading segment and whole cycle, respectively, both in terms of J/cm^3. Therefore, damage variables in loading and unloading segments could be obtained.

Since the dissipated energy of specimens under the amplitudes of 40 and 85 MPa was very small, there could be a great error in obtaining the damage variables in loading and unloading segments by the above method. Therefore, only the evolution processes of two types of damage variables with cycle number in cyclic loading segment at the amplitude of 130 MPa are shown in Fig. 7. As can be seen in Fig. 7, the damage ratio between loading and unloading segments was from 0.644 to 0.833 when dissipated energy density was used for definition with the average value of about 0.8. When AE counts were used for definition, the damage ratio was from 0.670 to 0.403 with the average of about 0.5. In the 5th to 9th cycles, the damage in loading segment was lower than that in unloading segment. It was seen that, although the overall change trends of the two types of damage variable in the

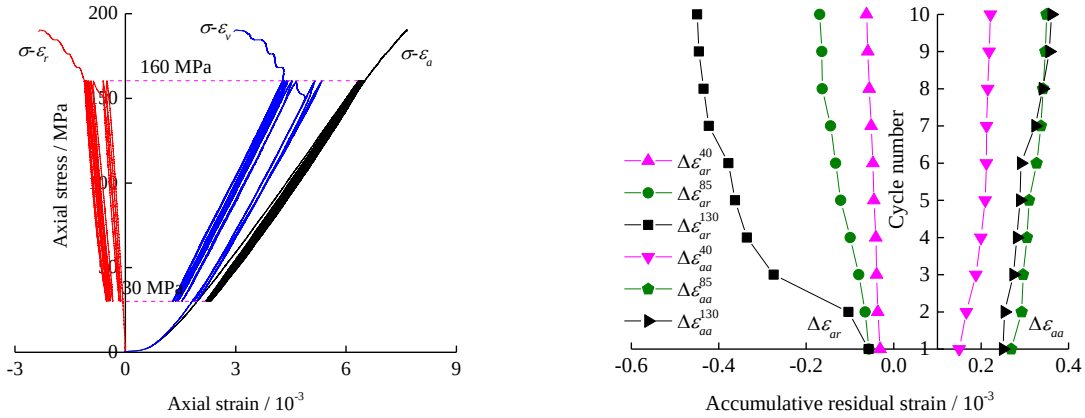

(a) Stress-strain curve

(b) Relationship between accumulative residual strain $\Delta\varepsilon_a$ and cycle number n

Fig. 8 Axial and radial deformation characteristics of limestone specimens

whole cyclic loading segment were basically the same at the amplitude of 130 MPa, damage in loading and unloading segments were different. Damage in loading segment defined by dissipated energy density was higher than that defined by AE counts.

4. Discussion

In summary, at the amplitudes of 40 and 85 MPa, the damage obtained from the two methods were inconsistent. For example, at the amplitude of 85 MPa, damage variables defined by AE counts were sharply increased in the 4th and 5th cycles, but those defined by dissipated energy density were almost equal in each cycle. In fact, this difference was related to the deformations and failure characteristics of the specimens used in this experiment. In the following, an analysis on this phenomenon based on axial and radial deformation characteristics is discussed.

Under cyclic loading, specimens produced certain plastic strains in each cycle, resulting in hysteresis curves, as shown in Fig. 8(a). In the deformation and failure processes of limestone specimens, the variations of axial stiffness were very small and failure was characterized by elastic-brittle splitting. Under high amplitude loads, radial strain hysteretic curve was sparser than that of axial strain and specimens showed obvious radial plastic deformation characteristic near failure.

The variation of residual strain of specimen with cycle number is shown in Fig. 8(b). At the amplitude of 40 MPa, accumulative axial ($\Delta\varepsilon_{aa}$) and residual ($\Delta\varepsilon_{ar}$) strains were smaller and tended to stabilize with cycle number. At the amplitude of 85 and 130 MPa, there were little differences in the $\Delta\varepsilon_{aa}$ of specimens (there was discreteness in specimens), but radial residual strain $\Delta\varepsilon_{ar}^{130}$ was much larger at the amplitude of 130 MPa. It was seen that the radial deformation of specimen was obviously more unstable than axial deformation. It was also seen from the fracture and morphology of specimens that, during axial compression, radial deformation at small load levels was very small (Poisson's ratio was only about 0.10). However, when stress was close to the peak value of specimen, new cracks were more likely to initiate and propagate along axial direction and form damage failure surfaces approximately parallel to the axial direction of specimens, the formation of damage failure surfaces could certainly create AE phenomena.

It is easy to understand that, unlike horizontal and inclined cracks, vertical cracks had little effects on axial deformation, Therefore, under the three amplitudes, the axial residual strains were stable with small ranges of variation and AE phenomena were mainly caused by the radial deformation damage of specimens. For example, at the amplitude of 85 MPa, the increase of radial residual strain in the 4th and 5th cycles was larger, which corresponded to the sudden increase of AE counts, but the increase of axial strain was not obvious. At the amplitude of 130 MPa, the third cycle also showed this pattern. It was obvious that, the axial and radial residual strains of cyclic loading segment were both small and there was almost no AE phenomena at the load amplitude of 40 MPa. Therefore, the variation of AE counts was not consistent with residual axial deformation and dissipated energy density during the compression of specimens.

It was seen that the damage value of cyclic loading segment under low stress level was larger when damage variable was defined by dissipated energy density for limestone specimens in this test. Even though the damage of specimen under the load amplitude of 130 MPa was basically the same as that defined by AE counts, it did not accurately reflect the radial deformation damage characteristics of the specimens. Therefore, it was more practical to define limestone specimen damage variable from the perspective of AE counts and it could realize the continuous characterization of cyclic loading segment specimen damage.

Section 3.3 showed that damage occurred in both loading and unloading segments. However, the damage mechanism of specimens in loading and unloading segments were different. From the perspective of energy, a reasonable analysis of damage mechanism could be performed. During loading process, press continued to work on specimens and energy was gradually accumulated in which the degree of accumulative energy near specimen defect was high. When accumulative energy around defect

area exceeded energy storage limit, local damage was first occurred and then energy was released further expanding the defect. As loading continued, energy was once more accumulated near the expanded defect and released creating damage. In continuous process, damage range was further expanded (the damage surface of limestone specimens was mainly axial in this test), until loading segment was completed. The released energy was dissipated and the remaining energy was stored in specimen in the form of elastic energy. During unloading process, accumulative elastic energy in the loading segment of specimens began to release to a steady state. Poisson effect slowly recovered radial deformation with the axial rebound of specimens and the damage surface formed by loading segment was squeezed and staggered during this process, which aggravated damage. In addition, reflected tensile waves formed in specimens during elastic energy release process also generated damage (Yan *et al.* 2016). As cycle number was increased, damage was gradually accumulated. In short, some damage occurred in loading and unloading segments and it was more significant under high stress amplitudes.

It was seen that, during the excavation and unloading of deep rock masses, not only the effect of the abutment pressure of surrounding rocks in tunnel due to excavation on the damage and failure of rock masses, but the damage of local rock masses caused by stress removal and strain recovery had to be taken into account, especially when the stress state of surrounding rocks is close to the ultimate strength of specimen.

5. Conclusions

- Under lower amplitude cyclic loads, the dissipated energy density of each cycle was gradually decreased with the increase of cycle number and AE counts were very few. At higher amplitude loads, the dissipated energy density of each cycle was basically the same at the same amplitude and AE counts were sharply increased near the peak value of cyclic loading. When the upper limit of cyclic loading was close to specimen strength, AE counts in each cycle showed a uniform and stable development trend, and felicity effect was obvious.
- The unstable characteristics of radial deformation of rock specimens limited the definition of dissipated energy density and damage variables of cyclic loading and unloading segments were larger at lower loading amplitudes. The two types of damage proportions of loading and unloading segments were different and the damage variable defined by dissipated energy density was less than that defined by AE counts.
- At high stress levels, the damage value of unloading segment of limestone specimens was more significant in the process of cyclic loading. During the excavation of deep rock masses, the damage caused by the deformation recovery of rock masses during unloading had to be considered and the overall damage of surrounding rock masses had to be minimized by setting reasonable construction parameters.

Acknowledgments

The research described in this paper was financially supported by the National Natural Science Foundation of China (No. 52074009) and the Anhui Provincial Ntaural Science Foundation (2208085QE174) and the Open Research Fund of the State Key Laboratory of Coal Resources and safe Mining, CUMT (SKLCRSM22KF017).

References

Bahrani, N., Valley, B. and Kaiser, P. (2019), "Influence of stress path on stress memory and stress fracturing in brittle rocks", *Can. Geotech. J.*, **56**(6), 852-867. https://doi.org/10.1139/cgj-2018-0291.

Castagna, A., Ougier-Simonin, A., Benson, P.M., Browning, J., Walker, R.J., Fazio, M. and Vinciguerra, S. (2018), "Thermal damage and pore pressure effects of the brittle-ductile transition in comiso limestone", *J. Geophys. Res-Solid. Earth*, **123**(9), 7644-7660. https://doi.org/10.1029/2017JB015105.

Chen, J., Du, C., Jiang, D.Y., Fan, J.Y. and He, Y. (2016), "The mechanical properties of rock salt under cyclic loading-unloading experiments", *Geomech. Eng.*, **10**(3), 325-334. https://doi.org/10.12989/gae.2016.10.3.325.

Chu, Y.P., Sun, H.T. and Zhang, D.M. (2019), "Experimental study on evolution in the characteristics of permeability, deformation, and energy of coal containing gas under triaxial cyclic loading-unloading", *Energy Sci. Eng.*, **7**(5), 2112-2123. https://doi.org/10.1002/ese3.417.

Diederichs, M.S., Kaiser, P.K. and Eberhardt, E. (2004), "Damage initiation and propagation in hard rock during tunnelling and the influence of near-face stress rotation", *Int. J. Rock Mech. Min.*, **41**(5), 785-812. https://doi.org/10.1016/j.ijrmms.2004.02.003.

Fuenkajorn, K. and Phueakphum, D. (2010), "Effects of cyclic loading on mechanical properties of Maha Sarakham salt", *Eng. Geol.*, **112**(1-4), 43-52. https://doi.org/10.1016/j.enggeo.2010.01.002.

Ghamgosar, M., Erarslan, N. and Williams, D.J. (2017), "Experimental investigation of fracture process zone in rocks damaged under cyclic loadings", *Exp. Mech.*, **57**(1), 97-113. https://doi.org/10.1007/s11340-016-0216-4.

Jin, P.J., Wang, E.Y., Liu, X.F., Huang, N. and Wang, S.H. (2013), "Damage evolution law of coal-rock under uniaxial compression based on the electromagnetic radiation characteristics", *Int. J. Min. Sci. Technol.*, **23**(2), 213-219. https://doi.org/10.1016/j.ijmst.2013.04.017.

Kim, J.S., Lee, K.S., Cho, W.J., Choi, H.J. and Cho, G.C. (2015), "A comparative evaluation of stress-strain and acoustic emission methods for quantitative damage assessments of brittle rock", *Rock Mech. Rock Eng.*, **48**(2), 495-508. https://doi.org/10.1007/s00603-014-0590-0.

Li, D.X., Wang, E.Y., Kong, X.G., Jia, H.S., Wang, D.M. and Ali, M. (2019), "Damage precursor of construction rocks under uniaxial cyclic loading tests analyzed by acoustic emission", *Constr. Build. Mater.*, **206**, 169-178. https://doi.org/10.1016/j.conbuildmat.2019.02.074.

Li, Y.W., Zhao, Y.D., Tang, J.Z., Zhang, L.Y., Zhou, Y.Y., Zhu, X.Y., Jia, D. and Chen, M. (2020), "Rock damage evolution model of pulsating fracturing based on energy evolution theory", *Energy Sci. Eng.*, **8**, 1050-1067. https://doi.org/10.1002/ese3.567.

Liu, X.S., Ning, J.G., Tan, Y.L. and Gu, Q.H. (2016), "Damage constitutive model based on energy dissipation for intact rock subjected to cyclic loading", *Int. J. Rock Mech. Min.*, **85**, 27-32. https://doi.org/10.1016/j.ijrmms.2016.03.003.

Liu, Y., Dai, F., Dong, L., Xu, N.W. and Feng, P. (2018), "Experimental investigation on the fatigue mechanical properties of intermittently jointed rock models under cyclic uniaxial compression with different loading parameters", *Rock Mech. Rock Eng.*, **51**(1), 47-68. https://doi.org/10.1007/s00603-017-1327-7.

Naji, A.M., Emad, M.Z., Rehman, H. and Yoo, H. (2019), "Geological and geomechanical heterogeneity in deep hydropower tunnels: A rock burst failure case study", *Tunn. Undergr. Space Technol.*, **84**, 507-521. https://doi.org/10.1016/j.tust.2018.11.009.

Peng, K., Zhou, J.Q., Zou, Q.L. and Yan, F.Z. (2019), "Deformation characteristics of sandstones during cyclic loading and unloading with varying lower limits of stress under different confining pressures", *Int. J. Fatig.*, **127**, 82-100. https://doi.org/10.1016/j.ijfatigue.2019.06.007.

Qi, F.Z. and Ma, Z.G. (2019), "Investigation of the roof presplitting and rock mass filling approach on controlling large deformations and coal bumps in deep high-stress roadways", *Lat. Am. J. Solid. Struct.*, **16**(4), 1-24. http://dx.doi.org/10.1590/1679-78255586.

Qiu, S.L., Feng, X.T., Xiao, J.Q. and Zhang, C.Q. (2014), "An experimental study on the pre-peak unloading damage evolution of marble", *Rock Mech. Rock Eng.*, **47**(2), 401-419. https://doi.org/10.1007/s00603-013-0394-7.

Srinivasan, V., Gupta, T., Ansari, T.A. and Singh, T.N. (2020), "An experimental study on rock damage and its influence in rock stress memory in a metamorphic rock", *Bull. Eng. Geol. Environ.*, **79**(8), 4335-4348. https://doi.org/10.1007/s10064-020-01813-y.

Tang, J.H., Chen, X.D., Dai, F. and Wei, M.D. (2020), "Experimental investigation of fracture damage of notched granite beams under cyclic loading using DIC and AE techniques", *Fatig. Fract. Eng. Mater. Struct.*, **43**(7), 1583-1596. https://doi.org/10.1111/ffe.13253.

Voznesenskii, A.S., Kutkin, Y.O., Krasilov, M.N. and Komissarov, A.A. (2015), "The influence of the stress state type and scale factor on the relationship between the acoustic quality factor and the residual strength of gypsum rocks in fatigue tests", *Int. J. Fatig.*, **84**, 53-58. https://doi.org/10.1016/j.ijfatigue.2015.11.016.

Wang, Y.H., Liu, Y.F. and Ma, H.T. (2012), "Changing regularity of rock damage variable and resistivity under loading condition", *Saf. Sci.*, **50**(4), 718-722. https://doi.org/10.1016/j.ssci.2011.08.046.

Wang, Z.L., Li, Y.C. and Wang, J.G. (2008), "A method for evaluating dynamic tensile damage of rock", *Eng. Fract. Mech.*, **75**(10), 2812-2825. https://doi.org/10.1016/j.engfracmech.2008.01.005.

Xiao, F.K., He, J., Liu, Z.J., Shen, Z.L. and Liu, G. (2019), "Analysis on warning signs of damage of coal samples with different water contents and relevant damage evolution based on acoustic emission and infrared characterization", *Infrar. Phys. Technol.*, **97**, 287-299. https://doi.org/10.1016/j.infrared.2019.01.007.

Xiao, J.Q., Ding, D.X., Jiang, F.L. and Xu, G. (2010), "Fatigue damage variable and evolution of rock subjected to cyclic loading", *Int. J. Rock Mech. Min.*, **47**, 461-468. https://doi.org/10.1016/j.ijrmms.2009.11.003.

Xiao, J.Q., Feng, X.T., Ding, D.X. and Jiang, F.L. (2011), "Investigation and modeling on fatigue damage evolution of rock as a function of logarithmic cycle", *Int. J. Numer. Anal. Meth. Geomech.*, **35**, 1127-1140. https://doi.org/10.1002/nag.946.

Xie, H.P., Li, L.Y., Peng, R.D. and Ju, Y. (2009), "Energy analysis and criteria for structural failure of rocks", *J. Rock Mech. Geotech. Eng.*, **1**(1), 11-20. https://doi.org/10.3724/SP.J.1235.2009.00011.

Yan, P., Zhao, Z.G., Lu, W.B., Chen, M. and Zhou, C.B. (2016), "Factors influencing vibration effects induced by in-situ stress transient unloading of deep rock mass", *Rock Soil Mech.*, **37**(2), 545-553. https://doi.org/10.16285/j.rsm.2016.02.028.

Zhang, M., Dou, L.M., Konietzky, H., Song, Z.Y. and Huang, S. (2020), "Cyclic fatigue characteristics of strong burst-prone coal: Experimental insights from energy dissipation, hysteresis and micro-seismicity", *Int. J. Fatig.*, **133**, 105429. https://doi.org/10.1016/j.ijfatigue.2019.105429.

Zhou, X.P., Zhang, Y.X. and Ha, Q.L. (2008), "Real-time computerized tomography (CT) experiments on limestone damage evolution during unloading", *Theor. Appl. Fract. Mech.*, **50**(1), 49-56. https://doi.org/10.1016/j.tafmec.2008.04.005.

CC